Materials Science in Semiconductor Processing 122 (2021) 105493

Contents lists available at ScienceDirect

Materials Science in Semiconductor Processing

journal homepage: http://www.elsevier.com/locate/mssp

Synthesis of CdS and PbS nanoparticles by the thermal decomposition of ethyl xanthate complexes in castor oil using the heat-up technique

Michael B. Mensah [a], Johannes A.M. Awudza [a], Neerish Revaprasadu [b,*], Paul O'Brien [c]

[a] Department of Chemistry, Kwame Nkrumah University of Science and Technology, Private Mail Bag, Kumasi, Ghana
[b] Department of Chemistry, University of Zululand, Private Bag X1001, KwaDlangezwa, 3880, South Africa
[c] School of Chemistry, The University of Manchester, Oxford Road, Manchester, M13 9PL, UK

ARTICLE INFO

Keywords:
Nanoparticles
Castor oil
CdS
PbS
Heat-up synthesis

ABSTRACT

Castor oil contains a range of fatty acids of which a high proportion is ricinoleic acid. We report the syntheses of CdS and PbS nanoparticles by the thermal decomposition of ethyl xanthate complexes of cadmium and lead in castor oil using the heat-up synthesis technique. The castor-oil capped CdS nanoparticles showed cubic zinc blende and wurtzite crystal structures and displayed band gap range of 2.63–2.84 eV. The CdS formed near-spherical clusters of nanocrystals with average particle size of 6.78 (±1.89) nm. The castor-oil capped PbS nanoparticles showed a rocksalt crystal structure and displayed an average band gap of 0.85 eV. The PbS showed variety of morphologies of nanostructured particles ranging from rods to belts. The average width and length of the PbS nanobelts observed were 22.2 (±2.3) nm and 225.9 (±23.3) nm respectively.

1. Introduction

Vegetable oils (VOs) have attracted attention as alternative green coordinating solvents for nanoparticle synthesis due to their abundance and low-toxicity. They consist of triacylglycerides of long chain aliphatic fatty acids which are effective for tuning the size and morphology of nanoparticles. Notable examples of VOs used as solvents for syntheses of metal chalcogenide nanoparticles are olive oil, sunflower oil and castor oil [1–3]. Castor oil is inedible and a monohydroxy lipid which contains a high amount (90%) of ricinoleic acid (*12-hydroxy-9-cis-octadecenoic acid*) (Fig. 1). These properties make castor oil an effective green solvent for applications requiring highly stable and polar organic solvent-nanoparticles colloidal dispersions (e.g. lubricants) [4]. However, castor oil is highly viscous due to the formation of hydrogen bonding between the hydroxylated triglyceride molecules. This increases the steric hindrance of the oil leading to the formation of weakly bound dimers and trimmers of the original triglycerides, resulting in a very high viscosity of 260.4 cSt at 40 °C [5].

The underlying difficulty in using VOs as solvents is their high viscosity which makes them unattractive to the traditional hot-injection technique due to the poor solubility of the precursors in VOs at room temperature. Co-solvents are usually used in addition to VOs to reduce the viscosity, especially in the hot injection method. In this approach, the dual or single source precursors are injected into a coordinating solvent. Akhtar et al. [6] synthesized PbS nanoparticles by injecting a solution of trimethylsilyl sulfide dissolved in a mixture of olive oil and octadecene (4:1 v/v) into a hot solution of PbO dissolved in a mixture of olive oil, oleic acid and octadecene (12.5:1:1 v/v). The octadecene was added to reduce the viscosity of the olive oil in order to induce uniform nucleation of nanoparticles whilst the oleic acid was to dissolve the PbO. Employing a similar procedure, Nyamen et al. [7] produced CdS and PbS nanoparticles by injecting a solution of heterocyclic dithiocarbamate complexes of Cd and Pb in trioctylphosphine (TOP) into hot olive oil. However, the heat-up method requires no injection and viscous liquids such as VOs could be used without co-solvents.

The heat-up method has been applied for the syntheses of metal oxide nanoparticles [8]. In this method, the reagents, including the precursors and solvents required for synthesis are loaded into a three necked flask at room temperature. The system is then degassed and purged with inert gas for a period to remove residual water and oxygen and then heated to the required temperature at a constant heating and stirring rates. At this point, the system is allowed to react for an appropriate length of time and then cooled to room temperature for purification. Kim et al. [8] used this route to synthesize uniform sized quantum confined iron oxide nanoparticles with sizes less than 4 nm. They thermally decomposed the iron oleate complex at 250 °C (with

* Corresponding author.
E-mail address: RevaprasaduN@unizulu.ac.za (N. Revaprasadu).

https://doi.org/10.1016/j.mssp.2020.105493
Received 9 June 2020; Received in revised form 1 October 2020; Accepted 2 October 2020
Available online 10 October 2020
1369-8001/

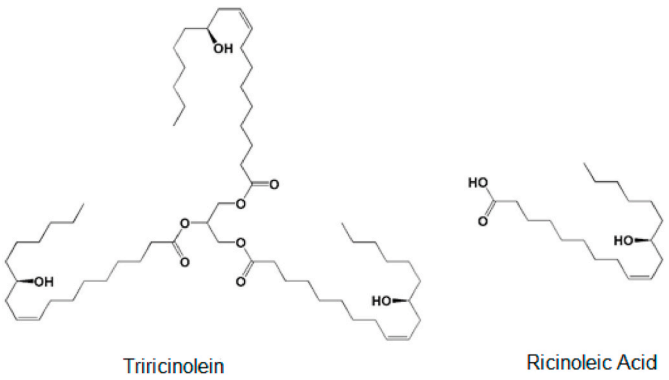

Fig. 1. Chemical structures of triricinolein and ricinoleic acid (major triacylglyceride and fatty acid in castor oil).

heating rate of 10 °C per minute) in oleyl alcohol for 30 min to form the iron oxide nanoparticles. Apart from metal oxides, the route has been attractive for the syntheses of metal chalcogenides nanoparticles. CdS, Cu_2S, ZnSe, ternary (Cu_2SnS_3) and quaternary nanomaterials ($CuInZn_xS_{2+x}$) have also been reported [9–13].

The difference between the hot-injection and heat-up methods lies in the procedure used to control the size and size distribution of the nanoparticles. The hot-injection route involves two major steps in controlling the distribution of nanoparticles, namely nucleation and crystal growth according to the LaMer model [14,15]. The sudden induction of burst nucleation due to high supersaturation introduced by the swift injection of precursors in hot solvent helps to initiate homogeneous nucleation leading to fairly uniform nanoparticles growth, thereby effectively controlling the size distribution. Similarly, the heat-up method also follows in two major steps which are the decomposition of the precursor and growth of the nanoparticles. The nanoparticles size distribution is controlled by the high energy barrier required for the induction of homogeneous nucleation. The nucleation is delayed until a large amount of monomers are accumulated by the decomposition of the precursor to reach a high supersaturation level where burst nucleation eventually evolves to initiate the nanoparticle growth stage. Thus, factors associated with size focusing such as no subsequent nucleation and high supersaturation level are fulfilled for narrowing of the nanoparticle size distribution [15].

Complexes of xanthates, thiobiurets, carbamates, thiosemicarbazides, dithiobiureas, thioureas, dithiophosphinates and N,N′-bis(thiocarbamoyl)hydrazines have been used as single source precursors (SSPs) for the syntheses of metal chalcogenide nanoparticles [16–22]. The advantages of SSPs over multiple source precursors are their low level of toxicity, ease of control of reaction stoichiometry and simplicity of handling because of their air-stability [23–27]. Amongst the various precursors, the xanthate complexes were used because of their clean decomposition at lower temperatures, as the by-products are highly volatile [28–30]. Infact, in the presence of amine ligands, they decompose easily even at room temperature [17]. Both CdS and PbS are important technological materials and their synthesis using low cost capping agents is highly desirable for their scalability for industrial applications. Herein, we have used the heat-up method as a facile technique for the syntheses of high quality CdS and PbS nanoparticles using ethyl xanthate complexes in castor oil. Phase pure nanoparticles were successfully prepared using cost effective capping agent *i.e.* castor oil, with tunable optical properties.

2. Experimental

2.1. Materials

Cadmium(II) acetate dihydrate (98%, Acros Organics), lead(II) acetate trihydrate (99.5–102.0%, Sigma-Aldrich), potassium ethyl xanthogenate (96%, Sigma-Aldrich), castor oil (Sigma-Aldrich), acetone (99% (GC), Honeywell, Riedel-de Haen), toluene (99.7% (GC), ACS reagent, Sigma-Aldrich) and methanol (99.8% (GC), ACS reagent, Sigma-Aldrich) were used as received.

2.2. Synthesis of cadmium(II) ethyl xanthate (1)

Cadmium(II) ethyl xanthate, $[Cd(S_2COEt)_2]$, was synthesized by reacting potassium ethyl xanthogenate (60 mmol, 9.62 g) and cadmium acetate dihydrate (30 mmol, 8.00 g) in water at room temperature. In the synthesis, 100 ml of aqueous solution of cadmium acetate dihydrate was added dropwise to 100 ml aqueous solution of potassium ethyl xanthogenate. See reaction scheme in Fig. 2. The resultant mixture was stirred for an hour to form water-insoluble precipitates of cadmium(II) ethyl xanthate. The precipitates were vacuum filtered and then dried in the fumehood overnight. The precipitates were further recrystallized in acetone and characterized. $[Cd(S_2COEt)_2]$: m.pt.: 165 °C, micro-elemental analysis calc. (found) (%): C 20.31 (20.38), H 2.84 (2.72), Cd 31.68 (31.16), S, 36.14 (36.02), significant IR (cm^{-1}): 2969 ν(C–H stretch), 1430–1360 ν(CH_2 and CH_3 deformation), 1180–571 ν(C=S, C–O and CH_2 rocking).

2.3. Synthesis of lead(II) ethyl xanthate (2)

Similarly lead(II) ethyl xanthate, $[Pb(S_2COEt)_2]$, was prepared by reacting lead acetate trihydrate (30 mmol, 11.38 g) and potassium ethyl xanthogenate (60 mmol, 9.62 g) in water at room temperature. The precipitates were filtered, dried, recrystallized in acetone and characterized. $[Pb(S_2COEt)_2]$: m.pt.: 132 °C, micro-elemental analysis, Calc. (found) (%): C 16.03 (16.19), H 2.24 (1.96), S 28.53 (28.44), Pb 46.10 (45.90). Significant IR (cm^{-1}): 2969 ν(C–H stretch), 1430–1360 ν(CH_2 and CH_3 deformation), 1180–571 ν(C=S, C–O and CH_2 rocking).

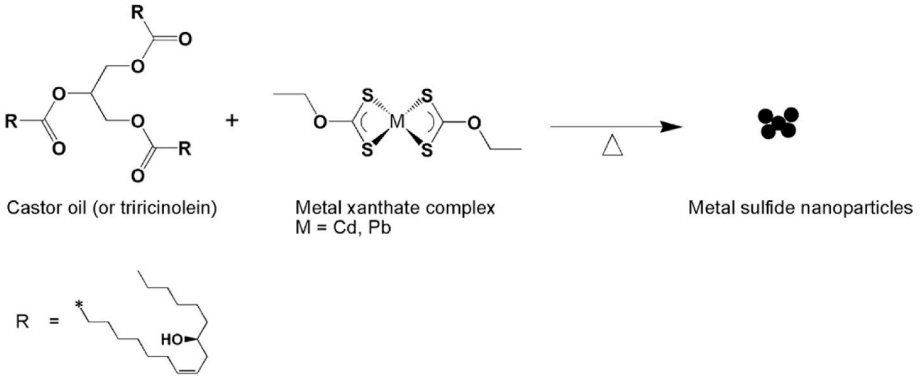

Fig. 2. Reaction scheme showing the synthesis of xanthate complexes (1) and (2).

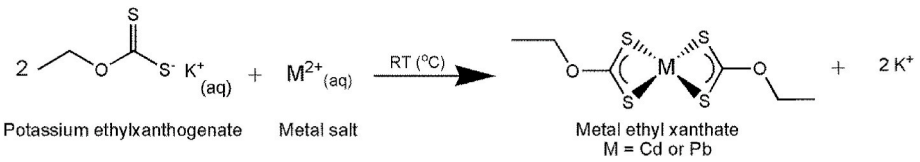

Fig. 3. Schematic diagram showing the syntheses of metal sulfides nanoparticles from ethyl xanthate complexes in castor oil.

2.4. Syntheses of CdS and PbS nanoparticles

The CdS and PbS nanoparticles were synthesized by the heat-up method employed by Shen et al. [31] with some modification. In a typical synthesis, 0.1 g of the precursor (0.282 mmol of $[Cd(S_2COEt)_2]$ or 0.222 mmol of $[Pb(S_2COEt)_2]$) and 5.0 ml castor oil were loaded into a three-necked flask at room temperature (Fig. 3). The system was then purged by degassing and bubbling with nitrogen for an hour at 100 °C with constant stirring (using a standard Schlenkline apparatus). The temperature was then increased at a rate of 15 °C min^{-1} and maintained at the target temperature for 15 min to allow decomposition and growth of nanoparticles. The reaction was quenched rapidly by cooling of the flask in a room temperature water bath followed by the addition of room temperature acetone when the reaction mixture reached 70 °C. The nanoparticles were purified by washing with methanol: toluene (7:1 v/v) solvent mixture three times, centrifuged and the final product dispersed in toluene for analyses.

The growth temperatures considered for CdS were 180, 200, 220, 240 and 280 °C and that of PbS was 140, 160, 180 and 200 °C. These temperatures were chosen based on the different decomposition patterns of the $[Cd(S_2COEt)_2]$ and $[Pb(S_2COEt)_2]$ precursors. The effect of time on nanoparticle growth was investigated by withdrawing aliquots of samples from the reaction mixture at 5, 10, 15, 30 and 60 min and analyzing them.

2.5. Characterization of complexes and nanoparticles

2.5.1. Xanthate complexes (1) and (2)

The melting points of the complexes (1) and (2) were determined with Barnstead Electrothermal melting point apparatus. The CHNS elemental analyses were measured using a PerkinElmer automated model 2400 series II CHNS/O analyzer. The metal analyses were done using ThermoiCap 6300 Inductively Coupled Plasma Optical Emission Spectroscopy (ICP-OES). Thermogravimetric analyses (TGA) of the complexes were carried out with a PerkinElmer Pyris 6TGA at heating rate of 10 °Cmin^{-1} under nitrogen gas and temperature range of 30–600 °C. The IR spectra (400–4000 cm^{-1}) of the complexes were measured with a Bruker FT-IR tensor 27 spectrophotometer.

2.5.2. Castor-oil capped CdS and PbS nanoparticles

The absorption spectra of the castor-oil capped CdS nanoparticles were obtained with a Varian Cary 50 UV–Visible spectrophotometer using a 1 cm path length quartz cuvette and toluene as a blank solvent. The near-infra red spectra of the castor-oil capped PbS nanoparticles were obtained with PerkinElmer UV/VIS/NIR spectrophotometer. Powder X-ray diffraction patterns were obtained with a Bruker AXS D8 diffractometer with nickel filtered Cu-Kα radiation (λ = 1.5418 Å, 40 kV, 40 mA, 2θ range (10–80°), with scan speed of 0.6. Micrographs were obtained using a JEOL 1010 Transmission Electron Microscope (TEM) with accelerating voltage of 100 kV and equipped with Megaview III camera and Soft Imaging Systems iTEM software. The TEM nanoparticle sizes and size distribution were analyzed with imageJ/Fiji software package. Philips XL-30 FEG Scanning Electron Microscope and Energy Dispersive X-ray Spectroscope (SEM/EDXS) equipped with DX4 detector was used to obtain the elemental composition of the nanoparticles. Prior to SEM/EDXS analyses, the nanoparticles were deposited on glass slides and coated using Edwards E306A coating system.

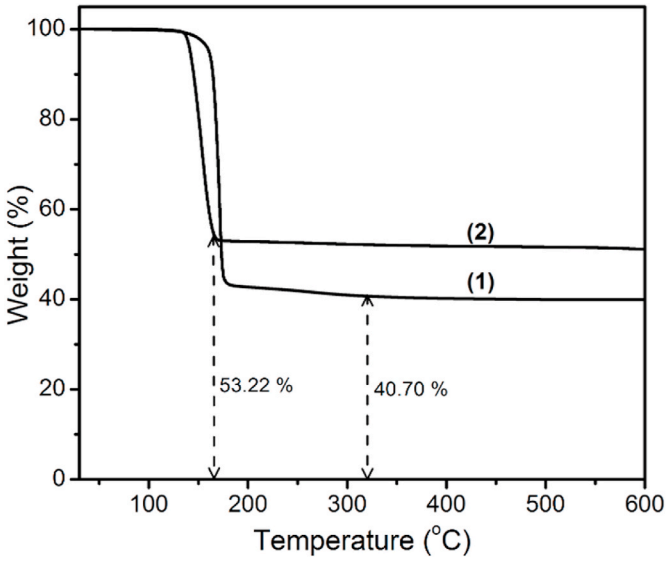

Fig. 4. TGA curves of cadmium(II) ethyl xanthate (1) and lead(II) ethyl xanthate (2) (at 30–600 °C under nitrogen, at heating rate of 10 °C min^{-1}).

3. Results and discussion

3.1. Thermal analyses of complexes

The TGA curves of the ethyl xanthate complexes of cadmium **(1)** and lead **(2)** from 30 to 600 °C at heating rate of 10 °Cmin^{-1} under nitrogen gas are shown in Fig. 4. The thermal analysis indicated a single step decomposition with the loss of $C_3H_5OS^{\bullet}$ and $S^{\bullet}$ moieties in both precursors. The expected residues from the decomposition process were CdS and PbS. The found percentage residues at 317 °C and 170 °C were 40.70% and 53.22% of the respective precursors and confirmed the formation of the desired products. Nair et al. [32] obtained similar TGA curve for cadmium ethyl xanthate complex.

The inflection point indicating the temperature at which there was intense decomposition of precursor was 171.45 °C for complex **(1)** whereas the onset and endset temperatures were 165.33 °C and 174.33 °C respectively. Similarly, the inflection point, onset and endset temperatures were 152.50 °C, 144.41 °C and 163.03 °C for complex **(2)** respectively. From the TGA analyses, it can be implied that more energy was required to increase the temperature of a unit mass of complex **(1)** to 1 °C than for **(2)**. Lead(II) ethyl xanthate easily gets heated, resulting in a quick decomposition compared to cadmium(II) ethyl xanthate.

3.2. CdS nanoparticles

3.2.1. p-XRD analysis

The p-XRD patterns for CdS nanoparticles synthesized at 200 and 280 °C using castor oil as both solvent and capping agent are shown in Fig. 5. The diffraction pattern of the CdS synthesized at 200 °C showed three major distinct peaks at 2θ values of 27.81°, 44.67° and 52.79° corresponding to (101), (110) and (201) planes of cubic crystal system (zinc blende structure) [32–34]. However, the p-XRD pattern also suggests a zinc blende/wurtzite polytypism nature of the CdS nanoparticles.

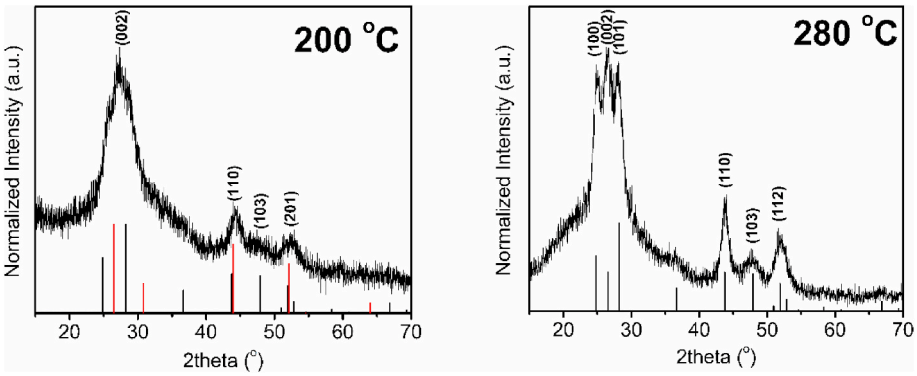

Fig. 5. p-XRD pattern of CdS nanocrystals synthesized by heating up cadmium ethyl xanthate in castor oil at 200 °C and 280 °C for 15 min (red lines: cubic (JCPDS no. 10–454); black lines: hexagonal (JCPD no. 6–314)). (For interpretation of the references to colour in this figure legend, the reader is referred to the Web version of this article.)

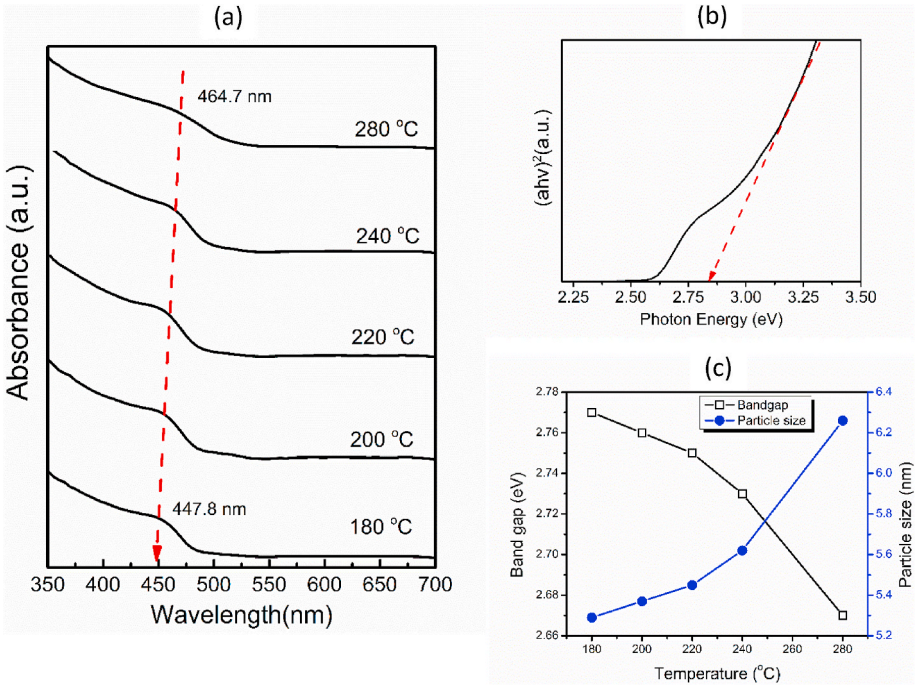

Fig. 6. (a) UV–Vis spectra and (b) Tauc plot of CdS nanocrystals synthesized at 180 °C by heating up of cadmium ethyl xanthate in castor oil for 15 min. (c) Plot of band gap energy and particle size against reaction temperature.

The XRD patterns for the CdS synthesized at 180 °C, 220 °C and 240 °C are shown in Figure S1.

The pattern for CdS synthesized at 280 °C had six diffraction peaks at 2θ values of 25.51°, 26.57°, 28.13°, 43.89°, 47.64° and 51.85° corresponding to the (100), (002), (101), (110), (103) and (112) planes suggesting a hexagonal or wurtzite crystal structure. The broad peaks suggest that the crystallite sizes were small demonstrating the effectiveness of the capping activity of the castor oil. The Scherrer calculated crystallite sizes (along the 101 plane) were 4.08 nm and 4.41 nm for CdS at the two different temperatures respectively. Nair et al. [32] reported Scherrer calculated crystallite size of CdS synthesized by thermolysis of cadmium ethyl xanthate at 280 °C for 1 h in TOPO to be 3.9 nm. This suggests that agglomeration of nanoparticles is quite faster in castor oil than in TOP/TOPO.

3.2.2. Optical properties

The optical spectra of the CdS nanocrystals synthesized in castor oil are shown in Fig. 6(a). As the temperature was increased from 180 to 280 °C, the absorption maximum shifted from 447.87 nm to 464.71 nm, indicative of a redshift (Fig. 6(a)). The band gap energies were estimated using the Tauc's relation [35]. The estimated band gap energy for CdS synthesized at 180 °C was 2.84 eV, higher than 2.42 eV for bulk CdS showing some level of quantum confinement (Fig. 6(b)).

The nanocrystal size was estimated using the Brus equation (1) [36]:

$$E_g^{nano} - E_g^{bulk} = \Delta E = \frac{h^2}{8r^2}\left[\frac{1}{m_e^*} + \frac{1}{m_h^*}\right] - \frac{1.8e^2}{4\pi\varepsilon\varepsilon_o r} - 0.248E_{RY}^* \quad (1)$$

where E_g^{nano} is band gap of the nanoparticle, E_g^{bulk} is band gap of bulk material, ΔE is the difference between the band gap of the bulk and nanomaterial, h is Plank's constant, r is radius of nanoparticle, m_e^* and m_h^* are effective masses of excited electron and hole, $\varepsilon$is relative permittivity, $\varepsilon_o$is permittivity of vacuum and $E_{RY}^*$is the Rydberg Energy.

The calculated energy band gaps and nanocrystal sizes of the CdS samples against reaction temperature are shown in Fig. 6(c). From Fig. 6 (a), the absorption maximum shifted from lower wavelength to higher wavelength as the temperature was increased. This observation

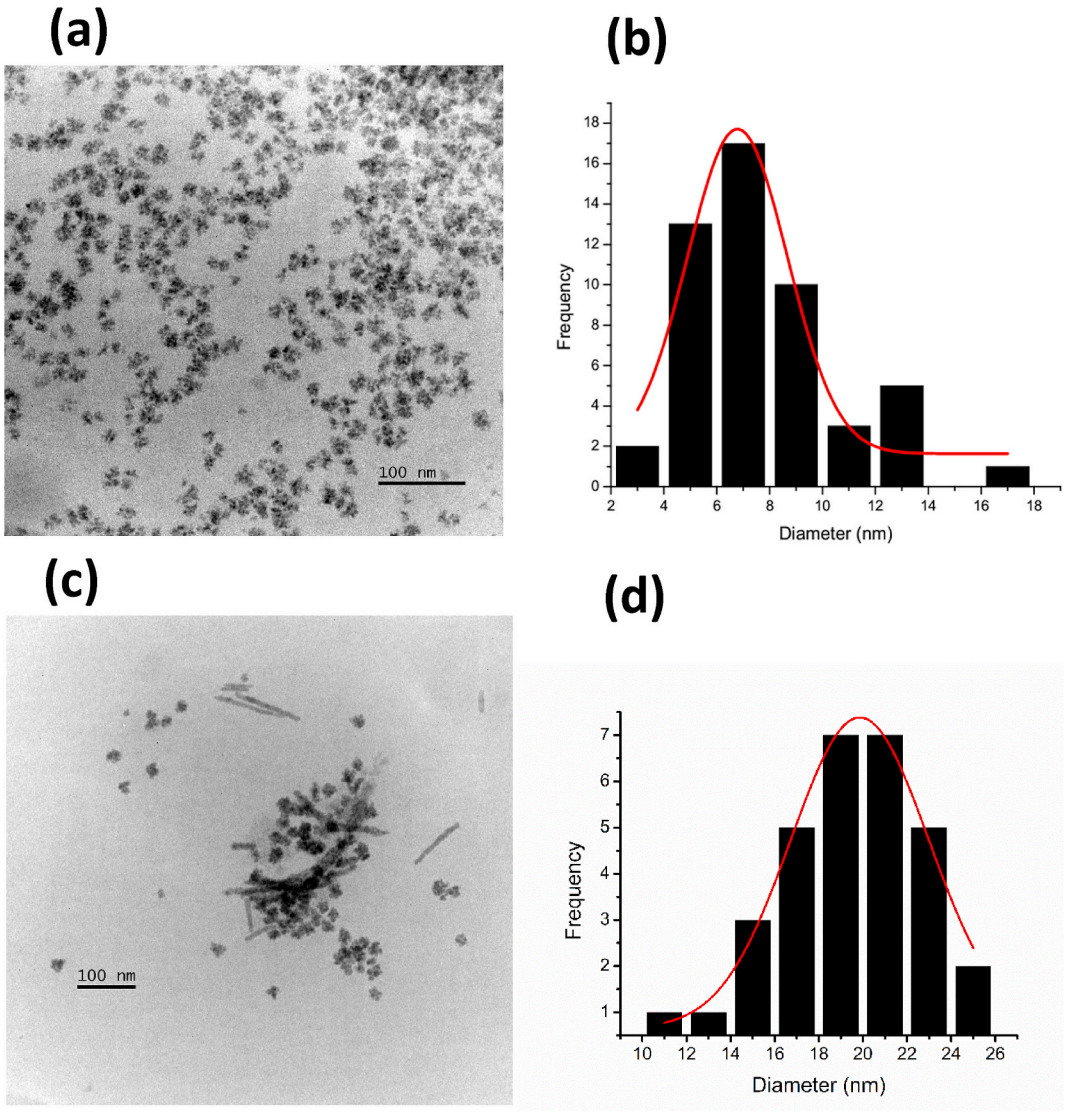

Fig. 7. TEM images and particle size distribution histograms of CdS nanoparticles synthesized at ((a) and (b)) 200 °C and ((c) and (d)) 280 °C via heating up cadmium ethyl xanthate in castor oil for 15 min, respectively.

confirmed the fact that increasing temperature usually leads to increasing particle size and decreasing band gap energy (Fig. 6(c)). The Scherrer calculated nanocrystallite sizes obtained from the XRD patterns were about 24% lower than those obtained from the Brus equation which suggests that the particle sizes could be made up of a number of crystallites. Increasing the time of reaction from 5 to 60 min and concentration of precursor from 0.02 to 0.08 g/ml (at 200 °C) did not show significant effect on the absorption maxima.

3.2.3. Morphology

The TEM micrographs and particle size distribution histogram of CdS nanoparticles synthesized at 200 °C showed interesting morphology (Fig. 7(a) and (b), Figure S2). The average particle size was found to be 6.78 (±1.89) nm which is about 22% higher than the 5.37 nm found using the Brus equation (1). The particles are near-spherical in shape in the form of nanoclusters. The polydispersity was calculated to be 27.88% which indicated that the particles sizes were uniform with the majority in the range of 6–8 nm (Fig. 7(c)). Increasing the temperature to 280 °C, an average particle size of 19.85 nm was obtained, with some formation of nanorods ranging 44.73–115.44 nm in length (Fig. 7(c) and (d), Figure S2). Shombe et al. [37] thermolyzedpiperidine and tetrahydroquinolinedithiocarbamate complexes of Cd in castor oil and ricinoleic acid at 190–300 °C for 30–120 min using the hot-injection method. They similarly obtained spherical to oval shaped CdS nanoparticles with particle sizes within 10–22 nm. The nanocluster and rod morphologies were not observed in their work. The elemental analyses by SEM/EDXS showed that the CdS nanoparticles synthesized was made up of approximately 49.51% of Cd and 50.49% of S (Figure S3).

3.3. PbS nanoparticles

3.3.1. p-XRD analysis

The p-XRD patterns of PbS synthesized at 140 °C, 160 °C and 180 °C in castor oil are shown in Fig. 8. The p-XRD patterns were clean without any impurity peaks implying that there was complete decomposition of the lead(II) ethyl xanthate precursor to pure crystalline PbS nanoparticles. The diffraction pattern at each temperature showed nine distinct peaks at 2θ values of 25.63°, 29.73°, 42.84°, 50.8°, 53.26°, 62.4°, 68.72°, 70.82° and 78.79° assigned to the (111), (200), (220), (311), (222), (400), (331), (420) and (422) planes for cubic (halite) PbS. The average Scherrer calculated crystallite sizes using the full width at half maximum (FWHM) values of peaks at (111), (200) and (220) planes were within 19.74–26.19 nm. The d-spacing was found to 3.00 Å at all the temperatures along the (200) plane.

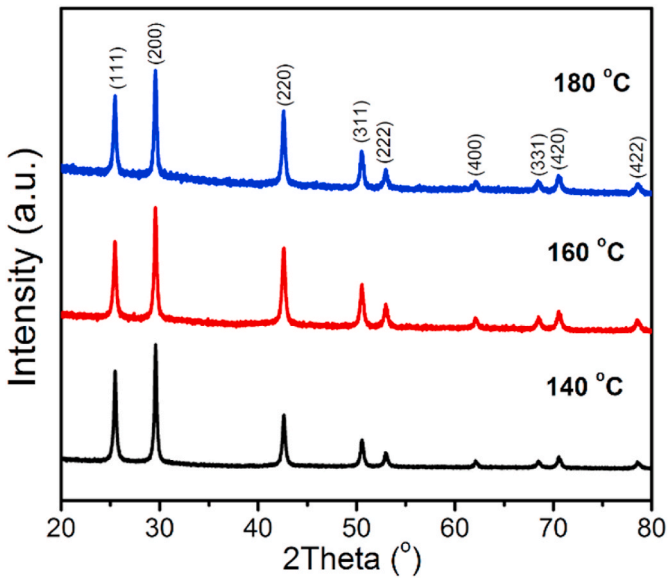

Fig. 8. p-XRD patterns of PbS nanoparticles synthesized by heating up lead(II) ethyl xanthate in castor oil at 140 °C, 160 °C and 180 °C for 15 min (JCPDS no. 78–1901).

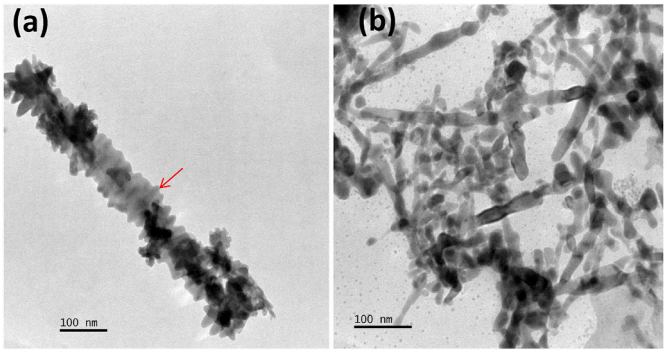

Fig. 9. TEM images of PbS synthesized at (a) 140 °C (showing nanoplates and rod) and (b) 200 °C (showing nanobelts) via heat-up of lead(II) ethyl xanthate in castor oil for 15 min.

3.3.2. Morphology

The morphologies of castor oil capped PbS synthesized at 140 °C and 200 °C are shown in Fig. 9. The morphology is a mixture of cubic, rod, belt and star shaped PbS nanoparticles.

The cubic morphology is common to PbS nanoparticles, however, rods made of plates, belts and stars are not usually observed. At 140 °C, the cubes were observed alongside packing of the square plates to form a rod (Fig. 9(a)). The nano-plates have average dimensions of 44.30 (±4.18) x 48.83(±2.33) nm whereas the rods had a length of 715 nm. At 200 °C, nanobelts and some cubes of PbS were obtained (Fig. 9(b)). The belts had an average width of 22.19(±2.33) nm and average length of 225.94(±23.32) nm. Star shaped morphology of PbS has been observed by Wang et al. [38], when they refluxed lead acetate trihydrate and thiourea in ethylene glycol at 197 °C for 3 h. They observed a cross shaped PbS consisting of six pods. Similarly, Phuruangrat and co-workers [39] also observed cubic and star-shaped dentritic PbS structures by a solvothermal reaction (using an autoclave) between lead nitrate and thiosemicarbazide in propylene glycol at 120 °C for 10 h. Sun et al. [40] also used a microwave-assisted method and obtained a flower-like PbS crystals by thermolyzing lead diethyldithiocarbamate in ethylenediamine. Jin et al. [41] prepared PbS of different morphologies including flowerlike, microsphere, multipod, six-armed star and truncated octahedron via citric acid assisted hydrothermal synthesis. It is worth mentioning that these different morphologies of PbS are common to growing PbS nanocrystals using the heat-up, refluxing and hydrothermal processes [42]. SEM-EDX elemental analysis showed that the PbS synthesized at 200 °C had a composition of 49.42% Pb and 50.58% S which indicates a very good stoichiometric proportions of the two elements (Figure S4).

3.3.3. Optical properties

The NIR spectra of PbS nanocrystals synthesized at 140 °C, 180 °C and 200 °C in castor oil are shown in Fig. 10(a). The narrow absorption peaks of PbS synthesized at 180 °C and 200 °C imply that the particle sizes may be uniformly distributed. The absorption maximum appeared at 1414 nm and by plotting the Tauc's plot (Fig. 10(b)) the band gaps were found to be 0.84, 0.85 and 0.86 eV at 140 °C, 180 °C and 200 °C respectively, which compare closely with 0.93 and 0.95 eV reported by Saah et al. [43,44] for nanostructured thin film and nanoparticles of PbS. There was little variation in the band gaps at the different temperatures which suggested that the lead(II) ethyl xanthate decomposed far too quickly before reaching the target temperatures. The average band gap (i.e. 0.85 eV) obtained for the PbS nanoparticles was about 107% higher than that of bulk PbS (i.e. 0.41 eV) implying that the castor oil was effective in tuning the band gap energy.

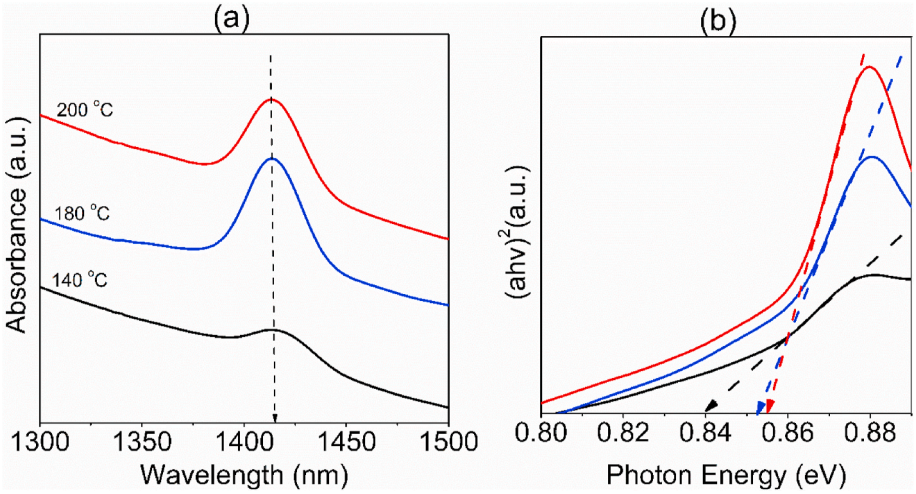

Fig. 10. NIR spectra (a) and Tauc's plot (b) of PbS nanocrystals synthesized at 140 °C, 180 °C and 200 °C via heating up in castor oil for 15 min.

4. Conclusions

The syntheses of CdS and PbS nanoparticles by the thermal decomposition of ethyl xanthate complexes in castor oil via the heat-up technique have been shown in this study. The complexes showed a single step decomposition pattern. A cubic zinc blende CdS was obtained at lower temperature (200 °C) and a hexagonal/wurtzite at higher temperature (280 °C). The band gap energies of the CdS nanoparticles were within 2.63–2.84 eV. The TEM images of the CdS showed average particle size of 6.78(±1.89) nm and clusters of spherical and rodlike particles. Rocksalt PbS nanoparticles was obtained in the form of nanobelts, rods, plates and star morphology. SEM/EDXS elemental analyses showed that the CdS and PbS nanoparticles had compositions of 49.74% Cd and 50.49% S and 49.42% Pb and 50.58% S respectively. The use of green solvents has the potential for large-scale synthesis of good quality semiconductor metal chalcogenide nanoparticles.

Author statement

Michael B.Mensah: Conceptualisation; methodology; formal analysis; writing original draft.

Johannes A. M. Awudza: Supervision; review and editing draft; funding acquisition.

Paul O'Brien: Supervision; review and editing draft; funding acquisition.

Neerish Revaprasadu: Supervision; review and editing draft; funding acquisition.

Data Availability Statement

The raw/processed data required to reproduce these findings cannot be shared at this time as the data also forms part of an ongoing study.

Declaration of competing interest

The authors declare that they have no known competing financial interests or personal relationships that could have appeared to influence the work reported in this paper.

Acknowledgement

The authors wish to thank The Royal Society, DFID, Africa Capacity Building Initiative for providing financial support for this project.

Appendix A. Supplementary data

Supplementary data to this article can be found online at https://doi.org/10.1016/j.mssp.2020.105493.

References

[1] S. Mondal, S. Bera, G. Narender, S. Ray, CdSe quantum dots-poly (3-hexylthiophene) nanocomposite sensors for selective chloroform vapor detection at room temperature, Appl. Phys. Lett. 101 (2012), 173108.
[2] A.S. Pereira, N.J. Silva, T. Trindade, S. Pereira, A single-source route for the synthesis of metal oxide nanoparticles using vegetable oil solvents, J. Nanosci. Nanotechnol. 12 (2012) 8963–8968.
[3] G.B. Shombe, E.B. Mubofu, S. Mlowe, N. Revaprasadu, Synthesis and characterization of castor oil and ricinoleic acid capped CdS nanoparticles using single source precursors, Mater. Sci. Semicond. Process. 43 (2016) 230–237.
[4] M. Lattuada, T.A. Hatton, Functionalization of monodisperse magnetic nanoparticles, Langmuir 23 (2007) 2158–2168.
[5] T.A. Isbell, Chemistry and physical properties of estolides, Grasas Y Aceites 62 (2011) 8–20.
[6] J. Akhtar, M.A. Malik, P. O'Brien, K. Wijayantha, R. Dharmadasa, S.J. Hardman, et al., A greener route to photoelectrochemically active PbS nanoparticles, J. Mater. Chem. 20 (2010) 2336–2344.
[7] L.D. Nyamen, N. Revaprasadu, P.T. Ndifon, Low temperature synthesis of PbS and CdS nanoparticles in olive oil, Mater. Sci. Semicond. Process. 27 (2014) 191–196.
[8] K.J. Klabunde, R.M. Richards, Nanoscale Materials in Chemistry, John Wiley & Sons, 2009, pp. 142–150.
[9] X. Liu, Y. Jiang, X. Lan, S. Li, D. Wu, T. Han, et al., Synthesis of high quality and stability CdS quantum dots with overlapped nucleation-growth process in large scale, J. Colloid Interface Sci. 354 (2011) 15–22.
[10] Y. Zhang, X. Li, W. Xu, S. Li, H. Wang, L.S. Li, The size controlled synthesis and self-assembled of monodisperse Cu_2S nanocrystals, Mater. Lett. 67 (2012) 117–120.
[11] K. Yu, A. Hrdina, X. Zhang, J. Ouyang, D.M. Leek, X. Wu, et al., Highly-photoluminescent ZnSe nanocrystals via a non-injection-based approach with precursor reactivity elevated by a secondary phosphine, Chem. Commun. 47 (2011) 8811–8813.
[12] H. Shen, H. Yuan, F. Wu, X. Bai, C. Zhou, H. Wang, et al., Facile synthesis of high-quality $CuInZn_xS_{2+x}$ core/shell nanocrystals and their application for detection of C-reactive protein, J. Mater. Chem. 22 (2012) 18623–18630.
[13] J.A. Adekoya, M.D. Khan, N. Revaprasadu, Phase transition in $Cu_{2+x}SnS_{3+y}$ ($0 \leq x \leq 2$; $0 \leq y \leq 1$) ternary systems synthesized from complexes of coumarin derived thiocarbamate motifs: optical and morphological properties, RSC Adv. 9 (2019) 35706–35716.
[14] J. Chang, E.R. Waclawik, Colloidal semiconductor nanocrystals: controlled synthesis and surface chemistry in organic media, RSC Adv. 4 (2014) 23505–23527.
[15] S.G. Kwon, T. Hyeon, Formation mechanisms of uniform nanocrystals via hot-injection and heat-up methods, Small 7 (2011) 2685–2702.
[16] N. Mintcheva, G. Gicheva, M. Panayotova, W. Wunderlich, A.A. Kuchmizhak, S. A. Kulinich, Preparation and photocatalytic properties of CdS and ZnS nanomaterials derived from metal xanthate, Materials 12 (2019) 3313.
[17] N. Mintcheva, G. Gicheva, M. Panayotova, S.A. Kulinich, Room-temperature synthesis of ZnS nanoparticles using zinc xanthates as molecular precursors, Materials 13 (2020) 171.
[18] G.B. Shombe, M.D. Khan, C. Zequine, C. Zhao, R.K. Gupta, N. Revaprasadu, Direct solvent free synthesis of bare α-NiS, β-NiS and α-β-NiS composite as excellent electrocatalysts: effect of self-capping on supercapacitance and overall water splitting activity, Sci. Rep. 10 (2020) 1–14.
[19] R. Akram, M.D. Khan, C. Zequine, C. Zhao, R.K. Gupta, M. Akhtar, et al., Cobalt sulfide nanoparticles: synthesis, water splitting and supercapacitance studies, Mater. Sci. Semicond. Process. 109 (2020), 104925.
[20] K.I. Ketchemen, M.D. Khan, S. Mlowe, L.D. Nyamen, P.T. Ndifon, P. O'Brien, et al., Tailoring shape and crystallographic phase of copper sulfide nanostructures using novel thiourea complexes as single source precursors, J. Inorg. Organomet. Polym. 29 (2019) 917–927.
[21] C. Gervas, M.D. Khan, S. Mlowe, C. Zhang, C. Zhao, R.K. Gupta, et al., Synthesis of off-stoichiometric CoS nanoplates from a molecular precursor for efficient H_2/O_2 evolution and supercapacitance, ChemElectroChem 6 (2019) 2560–2569.
[22] P.S. Nair, T. Radhakrishnan, N. Revaprasadu, G.A. Kolawole, P. O'Brien, Cd $(NH_2CSNHNHCSNH_2)Cl_2$: a new single-source precursor for the preparation of CdS nanoparticles, Polyhedron 22 (2003) 3129–3135.
[23] M.D. Khan, M. Aamir, M. Sohail, M. Sher, J. Akhtar, M.A. Malik, et al., Novel single source precursor for synthesis of Sb_2Se nanorods and deposition of thin films by AACVD: photo-electrochemical study for water reduction catalysis, Sol. Energy 169 (2018) 526–534.
[24] C. Gervas, M.D. Khan, C. Zhang, C. Zhao, R.K. Gupta, E. Carleschi, et al., Effect of cationic disorder on the energy generation and energy storage applications of $Ni_xCo_{3-x}S_4$ thiospinel, RSC Adv. 8 (2018) 24049–24058.
[25] M.D. Khan, M. Aamir, G. Murtaza, M.A. Malik, N. Revaprasadu, Structural investigations of $SnS_{1-x}Se_x$ solid solution synthesized from chalcogeno-carboxylate complexes of organo-tin by colloidal and solvent-less routes, Dalton Trans. 47 (2018) 10025–10034.
[26] M.D. Khan, M. Aamir, M. Sohail, M. Sher, N. Baig, J. Akhtar, et al., Bis (selenobenzoato) dibutyltin (iv) as a single source precursor for the synthesis of SnSe nanosheets and their photo-electrochemical study for water splitting, Dalton Trans. 47 (2018) 5465–5473.
[27] M.D. Khan, J. Akhtar, M.A. Malik, M. Akhtar, N. Revaprasadu, Phase-pure fabrication and shape evolution studies of SnS nanosheets, New J. Chem. 39 (2015) 9569–9574.
[28] M.D. Khan, M. Aamir, M. Sohail, S. Bhoyate, M. Hyatt, R.K. Gupta, et al., Electrochemical investigation of uncapped $AgBiS_2$ (schapbachite) synthesized using in situ melts of xanthate precursors, Dalton Trans. 48 (2019) 3714–3722.
[29] M.D. Khan, G. Murtaza, N. Revaprasadu, P. O'Brien, Synthesis of chalcopyrite-type and thiospinel minerals/materials by low temperature melts of xanthates, Dalton Trans. 47 (2018) 8870–8873.
[30] M.D. Khan, J. Akhtar, M.A. Malik, N. Revaprasadu, Tuning the phase and shape of copper sulfide nanostructures using mixed solvent systems, ChemistrySelect 1 (2016) 5982–5989.
[31] P.D. McNaughter, S.A. Saah, M. Akhtar, K. Abdulwahab, M.A. Malik, J. Raftery, et al., The effect of alkyl chain length on the structure of lead(II) xanthates and their decomposition to PbS in melt reactions, Dalton Trans. 45 (2016) 16345–16353.
[32] P.S. Nair, T. Radhakrishnan, N. Revaprasadu, G. Kolawole, P. O'Brien, Cadmium ethylxanthate: a novel single-source precursor for the preparation of CdS nanoparticles, J. Mater. Chem. 12 (2002) 2722–2725.
[33] J. Ouyang, M. Vincent, D. Kingston, P. Descours, T. Boivineau, M.B. Zaman, et al., Noninjection, one-pot synthesis of photoluminescent colloidal homogeneously alloyed CdSeS quantum dots, J. Phys. Chem. C 113 (2009) 5193–5200.
[34] R.R. Prabhu, M.A. Khadar, Characterization of chemically synthesized CdS nanoparticles, Pramana 65 (2005) 801–807.
[35] J. Tauc, R. Grigorovici, A. Vancu, Optical properties and electronic structure of amorphous germanium, Phys. Status Solidi B 15 (1966) 627–637.

[36] L.E. Brus, Electron–electron and electron-hole interactions in small semiconductor crystallites: the size dependence of the lowest excited electronic state, J. Chem. Phys. 80 (1984) 4403–4409.
[37] W.C.W. Chan, D.J. Maxwell, X. Gao, R.E. Bailey, M. Han, S. Nie, Luminescent quantum dots for multiplexed biological detection and imaging, Curr. Opin. Biotechnol. 13 (2002) 40–46.
[38] S.F. Wang, et al., Synthesis of cross-shaped PbS nanostructures by a surfactant-assisted reflux process, Mater. Lett. 60 (2006) 2759–2763.
[39] A. Phuruangrat, T. Thongtem, B. Kuntalue, S. Thongtem, Characterization of cubic and star-shaped dendritic PbS structures synthesized by a solvothermal method, Mater. Lett. 81 (2012) 55–58.
[40] J.Q. Sun, X.P. Shen, L.J. Guo, K.M. Chen, Q. Liu, Microwave-assisted synthesis of flower-like PbS crystals, Phys. E Low-Dimensional Syst. Nanostructures 41 (2009) 1527–1532.
[41] R. Jin, G. Chen, Q. Wang, J. Pei, J. Wang, L. Wang, Flowerlike PbS microcrystal: Citric acid assisted synthesis, shape evolution and electrical conductivities, Eur. J. Inorg. Chem. (2010) 5700–5708.
[42] M. Salavati-Niasari, D. Ghanbari, M.R. Loghman estarki, Star-shaped PbS nanocrystals prepared by hydrothermal process in the presence of thioglycolic acid, Polyhedron 35 (2012) 149–153.
[43] S.A. Saah, N.O. Boadi, C. Wilkins, Deposition of PbS thin films from lead hexadecyl and octyldecyl xanthate complexes using the spin coating method, MRS Adv. (2019) 733–742.
[44] S.A. Saah, M.D. Khan, P.D. McNaughter, J.A.M. Awudza, N. Revaprasadu, P. O'Brien, "Facile synthesis of $PbS_{1-x}Se_x$ ($0<x<1$) solid solution using bis(N,N-diethyl-N'-aphthoylchalcogenoureato)lead(II) complexes, New J. Chem. 42 (2018) 16602–16607.